THE ASTRONOMICAL JOURNAL, 126:385–392, 2003 July

HUBBLE SPACE TELESCOPE ACS CORONAGRAPHIC IMAGING OF THE CIRCUMSTELLAR DISK AROUND HD 141569A

M. CLAMPIN,[1] J. E. KRIST,[1] D. R. ARDILA,[2] D. A. GOLIMOWSKI,[2] G. F. HARTIG,[1] H. C. FORD,[2] G. D. ILLINGWORTH,[3] F. BARTKO,[4] N. BENÍTEZ,[2] J. P. BLAKESLEE,[2] R. J. BOUWENS,[3] T. J. BROADHURST,[5] R. A. BROWN,[1] C. J. BURROWS,[1] E. S. CHENG,[6] N. J. G. CROSS,[2] P. D. FELDMAN,[2] M. FRANX,[7] C. GRONWALL,[2] L. INFANTE,[8] R. A. KIMBLE,[7] M. P. LESSER,[9] A. R. MARTEL,[2] F. MENANTEAU,[2] G. R. MEURER,[2] G. K. MILEY,[7] M. POSTMAN,[1] P. ROSATI,[10] M. SIRIANNI,[2] W. B. SPARKS,[1] H. D. TRAN,[2] Z. I. TSVETANOV,[2] R. L. WHITE,[1] AND W. ZHENG[2]

Received 2002 December 12; accepted 2003 March 20

ABSTRACT

Multicolor coronagraphic images of the circumstellar disk around HD 141569A have been obtained with the *Hubble Space Telescope* Advanced Camera for Surveys. The *B*, *V*, and *I* images show that the disk's previously described multiple-ring structure is actually a continuous distribution of dust with a tightly wound spiral structure. Extending from the disk are two, more open spiral arms, one of which appears to reach the nearby binary star HD 141569BC. Diffuse dust is seen up to 1200 AU from HD 141569A. Although planets may exist in the inner region of the disk, tidal interaction with HD 141569BC seems more likely to be the cause of these phenomena. The disk appears redder than the star ($B-V = 0.21$ and $V-I = 0.25$), and its color is spatially uniform. A scattering asymmetry factor of $g = 0.25$–0.35 is derived. The azimuthal density distribution is asymmetric, varying by a factor of $\sim$3 at some radii.

Key words: circumstellar matter — stars: individual (HD 141569A) — stars: pre–main-sequence

1. INTRODUCTION

HD 141569A (spectral type B9.5 Ve; Jaschek & Jaschek 1992) is one of a few stars from which excess infrared radiation has been detected by the *Infrared Astronomical Satellite* (*IRAS*) and for which an associated circumstellar debris disk has been imaged in reflected light. Although HD 141569A was initially classified as an A-type shell star with infrared excess (Jaschek, Jaschek, & Egret 1986), it has properties common to both Herbig Ae/Be stars and young main-sequence stars (Fisher et al. 2000).

Images of HD 141569A's circumstellar disk show complex structure (Weinberger et al. 1999, hereafter W99; Augereau et al. 1999, hereafter A99) that might be attributed to gravitational perturbations by one or more planets (W99; Mouillet et al. 2001, hereafter M01). Other studies conclude that the 5 Myr old disk may be too young to have formed Jovian planets (Weinberger et al. 2000) and have proposed alternative sculpting mechanisms, such as dust migration (Takeuchi & Artymowicz 2001). The disk has a fractional infrared excess luminosity of $L_{\rm disk}/L_* = 8.4 \times 10^{-3}$, 3 times that of β Pic's disk (Sylvester et al. 1996), and has been imaged to a radius of $\sim$500 AU. At a distance of 99 pc (ESA 1997), the disk has an angular radius of 5″ and is therefore an ideal target for imaging with the *Hubble Space Telescope* (*HST*).

HST's Advanced Camera for Surveys (ACS) high resolution channel (HRC) features a coronagraph that suppresses the wings of the point-spread function (PSF) by factors of 5–10. When combined with reference PSF subtraction, the contrast between faint circumstellar material and the scattered light from a bright star can be improved by factors of 500–1000 (Krist et al. 2002) at a radial distance of 2″. The HRC coronagraph images of HD 141569A presented here show the complex structure of the disk with unprecedented resolution and provide new information about the disk's color.

2. OBSERVATIONS AND DATA REDUCTION

HD 141569A was observed with the HRC coronagraph on UT 2002 July 21 as part of the ACS Early Release Observation (ERO) program. The angular size of an HRC pixel is 0.″028 × 0.″025, and the FWHM of the unocculted coronagraphic field PSF is 0.″050 in the *V* band. The star was positioned behind the 1.″8 diameter occulting spot. A sequence of images was recorded over two orbits, after which *HST* was rolled by 28° and the sequence was repeated. This roll offset permits the distinction of PSF features, which are stationary with roll, from real disk structure, whose orientation on the detector changes with roll. Each sequence comprised the following filters and exposures: F435W (*B*), 1 × 150 s, 3 × 760 s; F606W (broad *V*), 1 × 100 s, 3 × 685 s; F814W (*I*), 1 × 100 s, 2 × 1200 s. The long exposures were not saturated, so the short ones were not used in our analysis.

The images were reduced using the standard techniques of bias and dark subtraction and division by a flat field.

[1] Space Telescope Science Institute, 3700 San Martin Drive, Baltimore, MD 21218.
[2] Department of Physics and Astronomy, Johns Hopkins University, 3400 North Charles Street, Baltimore, MD 21218.
[3] Lick Observatory, University of California at Santa Cruz, 1156 High Street, Santa Cruz, CA 95064.
[4] Bartko Science and Technology, P.O. Box 670, Mead, CO 80542.
[5] Racah Institute of Physics, Hebrew University, 91904 Jerusalem, Israel.
[6] NASA Goddard Space Flight Center, Greenbelt, MD 20771.
[7] Sterrewacht Leiden, Postbus 9513, NL-2300 RA, Leiden, Netherlands.
[8] Departamento de Astronomía y Astrofísica, Pontificia Universidad Católica de Chile, Casilla 306, Santiago, Chile.
[9] Steward Observatory, University of Arizona, 933 North Cherry Avenue, Tucson, AZ 85721.
[10] European Southern Observatory, Karl-Schwarzschild-Strasse 2, D-85748 Garching, Germany.

Because the coronagraphic spots shifted during launch, the prelaunch coronagraphic flat fields could not be applied directly to our images. Moreover, on-orbit flat fields were not available. Consequently, we constructed suitable flat fields by shifting the coronagraphic illumination pattern (including the occulting spot shadows) within the prelaunch flat fields. The flattened images were then combined using a standard cosmic-ray rejection algorithm.

The calibrated images of HD 141569A reveal the presence of the disk, but the coronagraphic PSF still dominates the images (Fig. 1). The coronagraph effectively suppresses the diffracted light below the level of scattered light caused by midfrequency surface errors in *HST*'s mirrors. The occulting spot itself diffracts light into a concentrated area around the perimeter of the imaged spot. Because the coronagraphic PSF is stable, most of this residual light can be subtracted using an image of a suitable reference star, improving the contrast.

Techniques for subtracting HRC coronagraphic PSFs are described by Krist et al. (2002) and summarized in the ACS Instrument Handbook (Pavlovsky et al. 2002). Because the positions of the occulting spots in the image plane are not static, optimal PSF subtraction can be achieved only when images of the target and spectrally similar reference stars are recorded contemporaneously. Previous studies of HD 141569A's disk with the Near Infrared Camera and Multi-Object Spectrometer (NICMOS; W99; A99) and the Space Telescope Imaging Spectrograph (STIS; M01) employed PSF subtraction, usually with a single reference star. W99 used three reference stars observed at various times and selected the one that provided the best subtraction. Because the ERO program produced the first on-orbit images taken with the HRC coronagraph, we are limited to using one set of reference-star images for PSF subtraction.

We observed the reference star HD 129433 immediately after HD 141569A. Both stars have the same spectral type, but HD 129433 is less reddened ($B-V=-0.01$ vs. 0.09). The images of HD 129433 were normalized to, aligned with, and subtracted from the corresponding images of HD 141569A (Figs. 1 and 2). Normalization and alignment of the HD 129433 images were achieved by simultaneously and iteratively scaling and shifting using cubic convolution interpolation. Convergence was achieved when the subtraction residuals were visually minimized. Alignment of the images is accurate to within ± 0.05 pixels ($\pm 0''.0013$). The normalizations of the corresponding images are accurate to within 2%. This normalization error corresponds to photometric errors of 0.02 and 0.1 mag arcsec^{-2} in the brightest and faintest regions of the disk, respectively. With only one available reference star, we cannot quantify the subtraction errors caused by mismatches of the stars' colors or time-dependent PSF variations.

The largest residuals in each PSF-subtracted image appear at the perimeter of the occulting spot, where the PSF is most sensitive to star-to-spot registration. These residuals force the exclusion of data within $\sim 1''.2$ (120 AU) of the star. Radial streaks caused by mismatches in registration, color, and focus also appear in the subtracted images. The F814W images are the most affected by residuals, probably because of large star-to-spot misalignments. After correcting for geometric distortion and rotating to a common orientation, the images for each filter were combined so that the final images reflected the smallest subtraction residuals from each of the constituent images (Fig. 3).

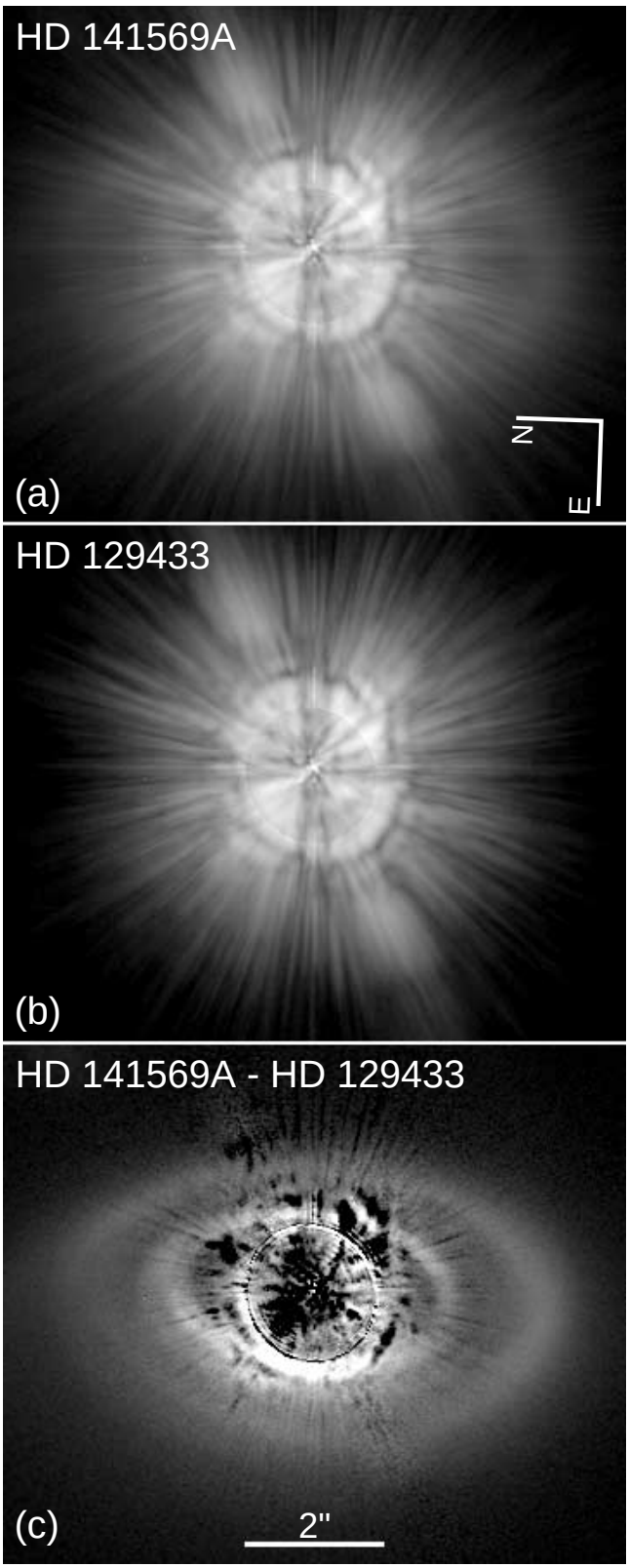

FIG. 1.—(*a*) HRC coronagraph image of HD 141569A through an F606W filter without PSF subtraction but corrected for geometric distortion. (*b*) Similar image of reference star HD 129433. (*c*) Image of HD 141569A's circumstellar disk after PSF subtraction. The images are displayed using a square-root stretch.

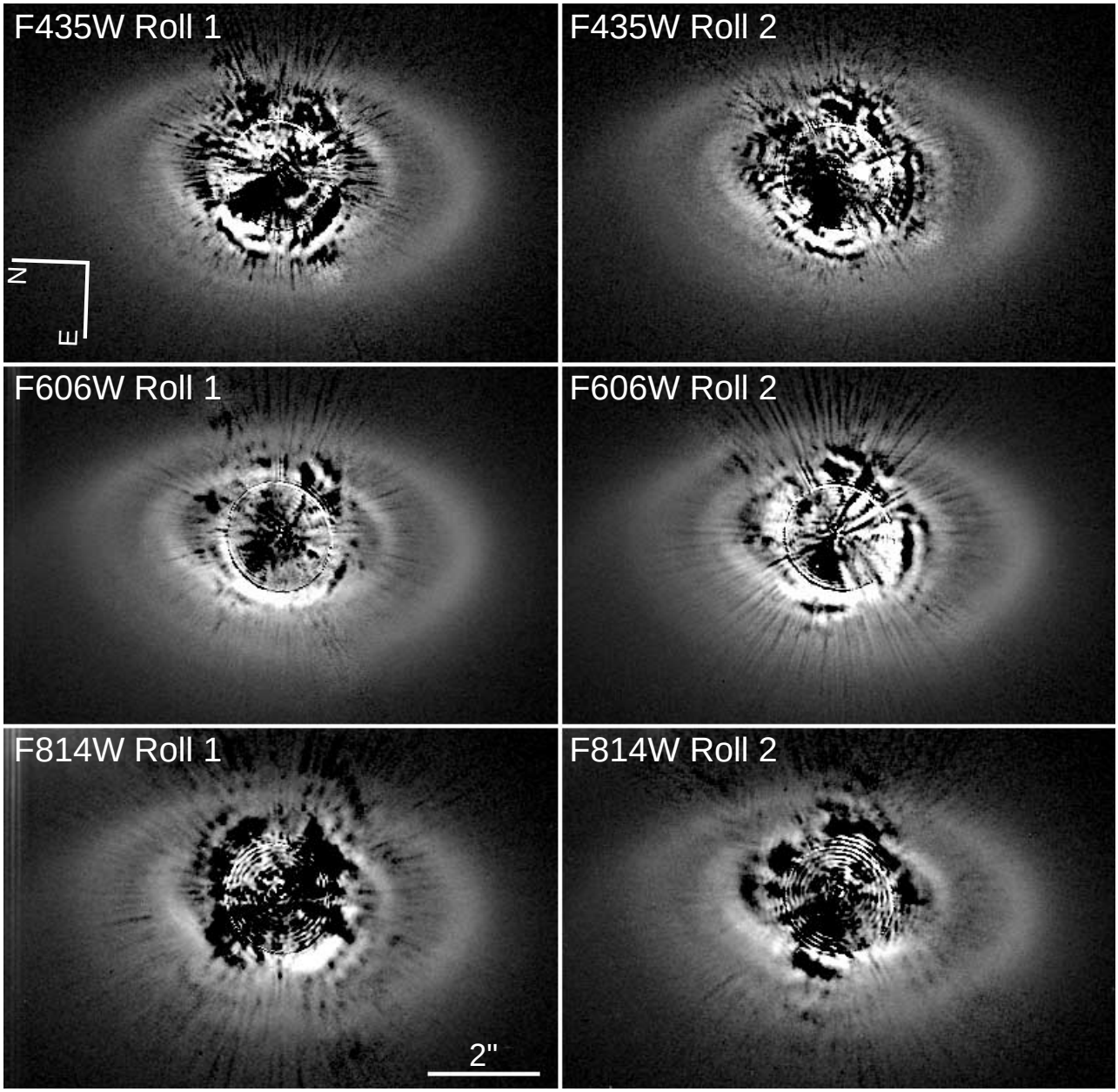

FIG. 2.—PSF-subtracted images of the disk obtained with three filters and two *HST* roll orientations. Images recorded at roll 2 have been rotated to the same orientation as the images recorded at roll 1. The images are displayed using a square-root stretch.

To derive the optical depth of HD 141569A's disk, the images must be normalized by the stellar flux. Unfortunately, it was not possible to obtain unsaturated images of HD 141569A and HD 129433 through HRC broadband filters. Consequently, we computed the flux from each star through each filter using the STSDAS synthetic photometry package SYNPHOT, which simulates most *HST* observing configurations. To approximate HD 129433's spectrum, we normalized Vega's spectrum to $V = 5.73$ (Hoffleit & Jaschek 1982) with $A_V = 0$ and assumed invariability. We also used Vega's spectrum for HD 141569A with $A_V = 0.34$ (Oudmaijer et al. 2001). Because HD 141569A is a known variable, we scaled its spectrum so that the ratio of the synthetic F606W fluxes of HD 141569A and HD 129433, f_{F606W}, was equal to the average brightness ratio of the aligned F606W coronagraphic PSFs of the two stars. The resulting magnitude for HD 141569A, $V = 7.18$, matches well the published measurement of de Winter et al. (2001). We then compared the ratios of the stars' flux ratios through different filters (e.g., $f_{\mathrm{F435W}}/f_{\mathrm{F814W}}$ and $f_{\mathrm{F606W}}/f_{\mathrm{F814W}}$) computed from the coronagraphic PSFs and from the synthetic spectra. The actual and synthetic flux ratios differed by less than 1%. This agreement indicates that the broadband colors of the synthetic spectra are well matched to the stars' colors and that the spectra can be used to produce accurate synthetic fluxes through the HRC filters. The PSF-subtracted images of the disk were normalized to the synthetic fluxes of HD 141569A, assuming a 52.5% throughput reduction caused by the coronagraph's Lyot stop.

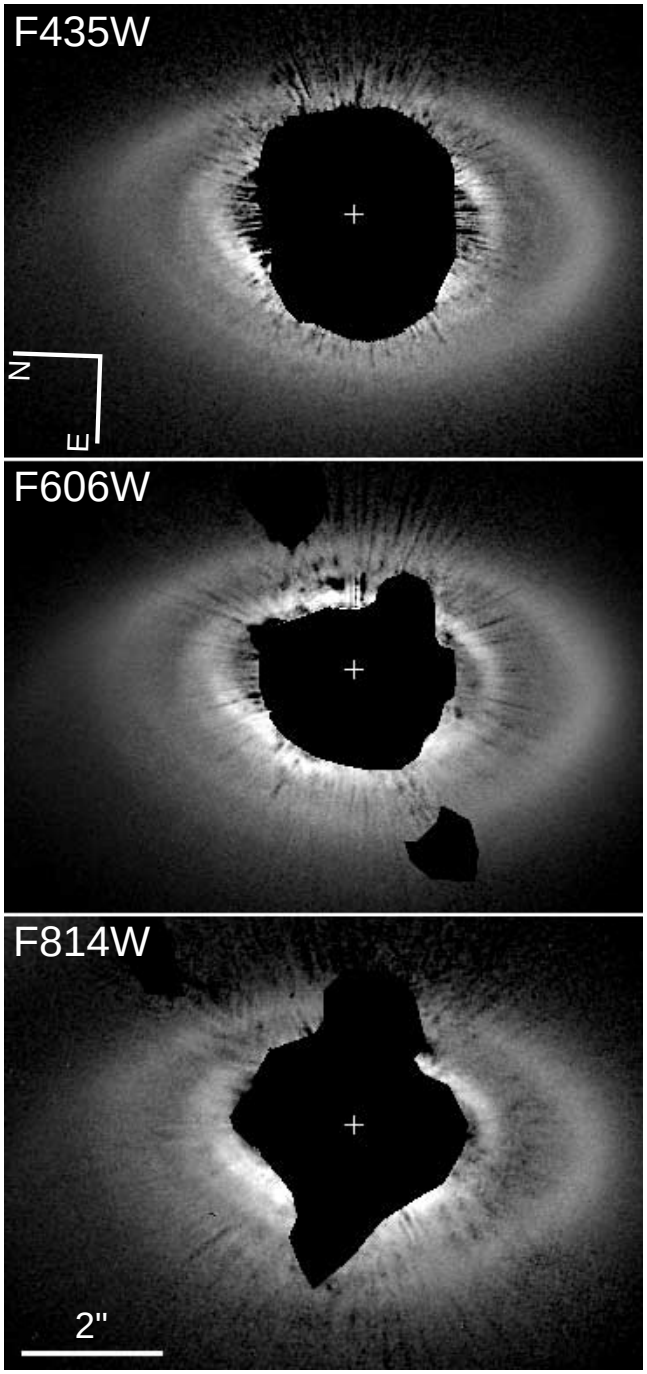

FIG. 3.—Images of the circumstellar disk after combining PSF-subtracted images from each roll orientation. The images are displayed using a square-root stretch. Regions containing large subtraction residuals are masked. The two black lobes in the F606W image mask residuals from the diagonal image artifact seen in Fig. 1 and discussed by Krist et al. (2002). The plus sign marks the measured position of the star.

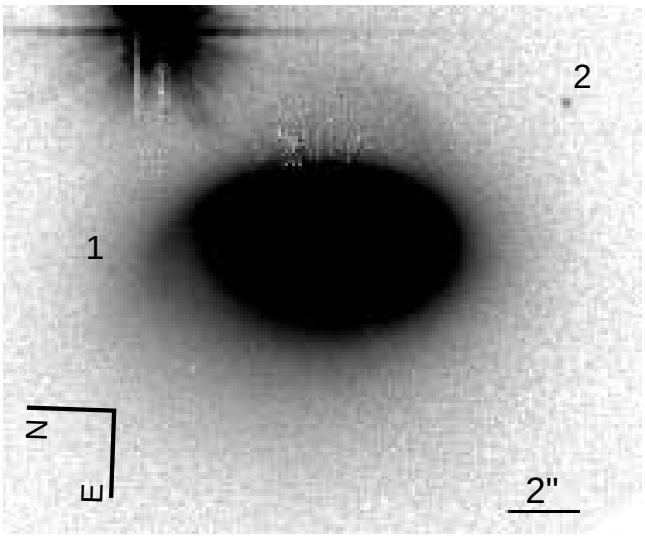

FIG. 4.—PSF-subtracted, combined F435W + F606W image of the disk, stretched to enhance the faint material extending from the front and back of the disk. Background stars 1 and 2 are labeled.

3. RESULTS

Our PSF-subtracted images yield a clearer and more detailed view of the disk than seen in previous *HST* images obtained with NICMOS (W99; A99) and STIS (M01). The disk has four distinct annular zones: an inner clearing within ~175 AU of the star, a bright "ring" with a sharp inner edge from ~175 to ~215 AU, a faint zone from ~215 to ~300 AU, and a broad "ring" from ~300 to ~400 AU. (All distances are measured along the disk's southern semimajor axis.) As shown in § 4, the inner and outer rings appear to be thin and tightly wound spirals of dust. Faint, broad arcs superposed upon fainter and more diffuse dust extend from the northeast and southwest regions of the disk (Fig. 4). The diffuse dust in the northeast extends ~1200 AU from HD 141569A. The arcs resemble open spiral arms, and the southwest one extends toward the binary star HD 141569BC, located ~8.″5 to the northwest of HD 141569A.

Figure 4 also shows two faint stars, labeled 1 and 2, located 6.″3 and 8.″0 from HD 141569A at position angles 12.°5 and 210.°0, respectively. Their V magnitudes are 25.5 ± 0.1 and 24.0 ± 0.1, respectively. Their colors are consistent with slightly reddened K stars or extincted, earlier-type stars, and we conclude that they are background stars.

Figures 5 and 6 show the V-band surface brightness of the disk, derived from the F606W images after azimuthal filtering (described below). The surface brightness ranges from 16.5 ± 0.02 mag arcsec^{-2} in the inner ring to 21.5 ± 0.1 mag arcsec^{-2} at the furthest extent of detection. Large azimuthal variations in the surface brightness of the disk are evident; the brightness of the outer ring varies by a factor of 2.5. The F814W/F606W and F814W/F435W ratios of the average surface brightness of the disk are $10\% \pm 0.7\%$ and $25\% \pm 2\%$ larger, respectively, than the corresponding flux ratios of HD 141569A. These ratios correspond to $B-V = 0.21$ and $V-I = 0.25$, which indicates that the disk is significantly redder than the star. There is no evidence of color variation across the disk above the levels set by the local PSF subtraction residuals.

The north-south orientation of the semimajor axis of the projected disk and the likely condition of forward scattering by dust (W99) imply that the brighter, eastern side of the disk is nearer to us. To investigate the scattering properties further, we created a composite image of the disk by summing the F435W and F606W images after normalizing them to a common average surface brightness. (Because the F814W image has relatively large PSF subtraction residuals, it was not included in the composite image.) Assuming that

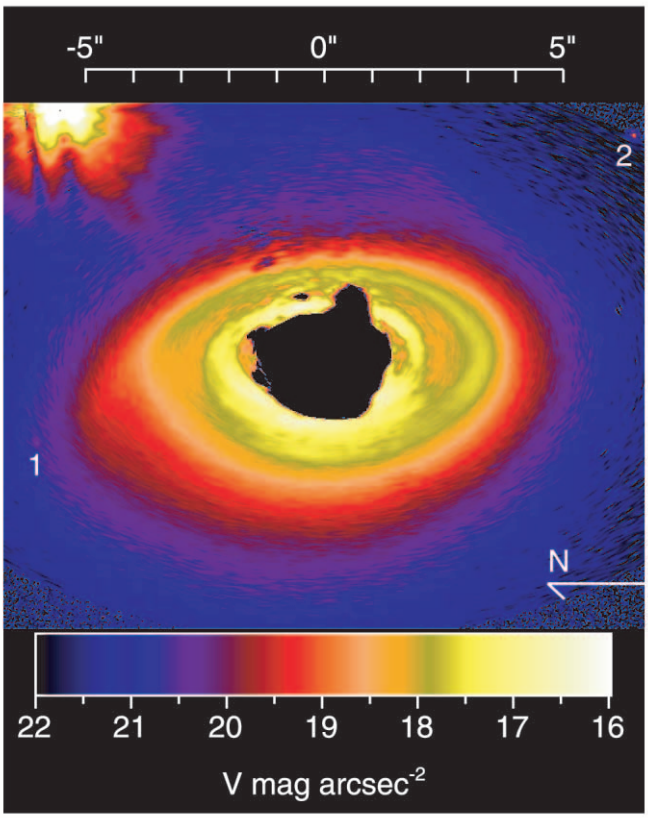

FIG. 5.—Color-coded map of the V-band surface brightness of the disk, obtained from the azimuthally filtered F606W image and photometrically calibrated from the synthetically derived flux of HD 141569A in this band. HD 141569BC lies in the upper left corner. Background stars are labeled 1 and 2. Note that the spatial scale is different from that of Fig. 4.

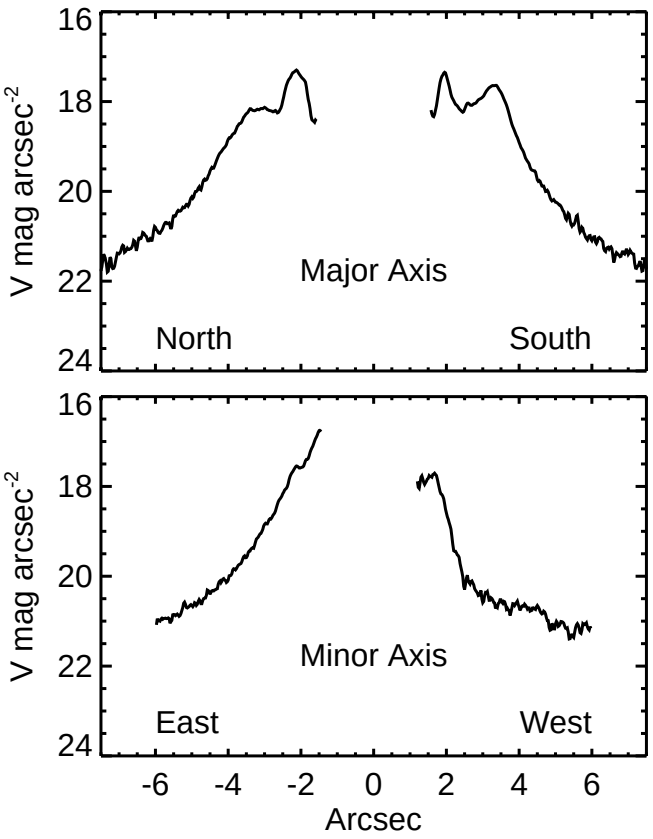

FIG. 6.—V-band surface brightness profiles along the major and minor axes of the disk, obtained from the azimuthally filtered F606W image and photometrically calibrated from the synthetically derived flux of HD 141569A in this band.

the disk is optically thin and flat and that it has an inclination angle of 55° from pole-on (M01), we deprojected the composite image to simulate a face-on view of the disk (Fig. 7*a*). The radial subtraction residuals seen in the constituent images (Fig. 2) were diminished by azimuthally filtering the combined image (Fig. 7*b*). Each pixel was replaced with the median value of a 7 pixel arc centered on the geometric center used in the deprojection procedure. This technique exploits the disk's slow azimuthal variations while preserving its more rapid radial ones. Each pixel in the azimuthally filtered image was then multiplied by the square of its distance from HD 141569A to compensate for the radially diminishing stellar illumination in the optically thin disk (Fig. 7*c*). The enhanced brightness of the near side of the disk and its symmetry along the line of sight as shown in this image indicate significant forward scattering of starlight by the dust.

W99 derived a scattering asymmetry parameter of $g = 0.11$ (Henyey & Greenstein 1941) for the disk, based on a measured east-west brightness ratio of 1.5 ± 0.2 and an assumption of azimuthally uniform disk density distribution. However, our images show that the disk is not azimuthally uniform. Consequently, we visually fitted a Henyey-Greenstein phase function to our entire deprojected F435W + F606W image, accounting for the inclination. We adjusted g until the region of symmetric brightness enhancement along the disk's near side was made consistent with the overall azimuthal brightness trend (Fig. 7*d*). We obtained satisfactory results for $g = 0.25$–0.35, which is consistent with the results of M01. Because the color of the disk appears uniform, this range of g is valid for all visual wavelengths. Depending on the infrared properties of the dust, g may decrease for wavelengths longer than 1.0 μm. For example, isotropic scattering ($g = 0$) would explain the brighter western side of the disk in 1.6 μm images obtained with NICMOS (A99).

Figure 7*d* maps the product of the dust's albedo (ω) and its optical depth perpendicular to the plane of the disk ($\tau_\perp$). This is proportional to $\kappa_s \Sigma$, where κ_s is the scattering opacity and Σ is the surface mass density of the dust. The map of $\omega\tau_\perp$ enhances the features within the disk, especially the tightly wound spiral structure of the inner and outer rings. These tight spirals and the broad, open spiral arms extending beyond the outer ring are traced in Figure 8. The outer ring unwinds counterclockwise, circumscribing about 450° of arc. The spiral overlaps itself in the northeast with a separation of ~80 AU. It also splits into the open spiral arms in the northeast and southwest. The inner ring also unwinds counterclockwise and overlaps itself from northeast to southeast. This spiral appears to merge with the outer spiral in the southeast, thereby filling the previously described gap between the inner and outer rings about 250 AU from the star. The interior of the inner ring appears relatively devoid of dust.

Figure 9 is a color-coded version of Figure 7*d*, with an expanded field of view and a calibrated brightness scale. Assuming κ_s is uniform throughout the disk (consistent with

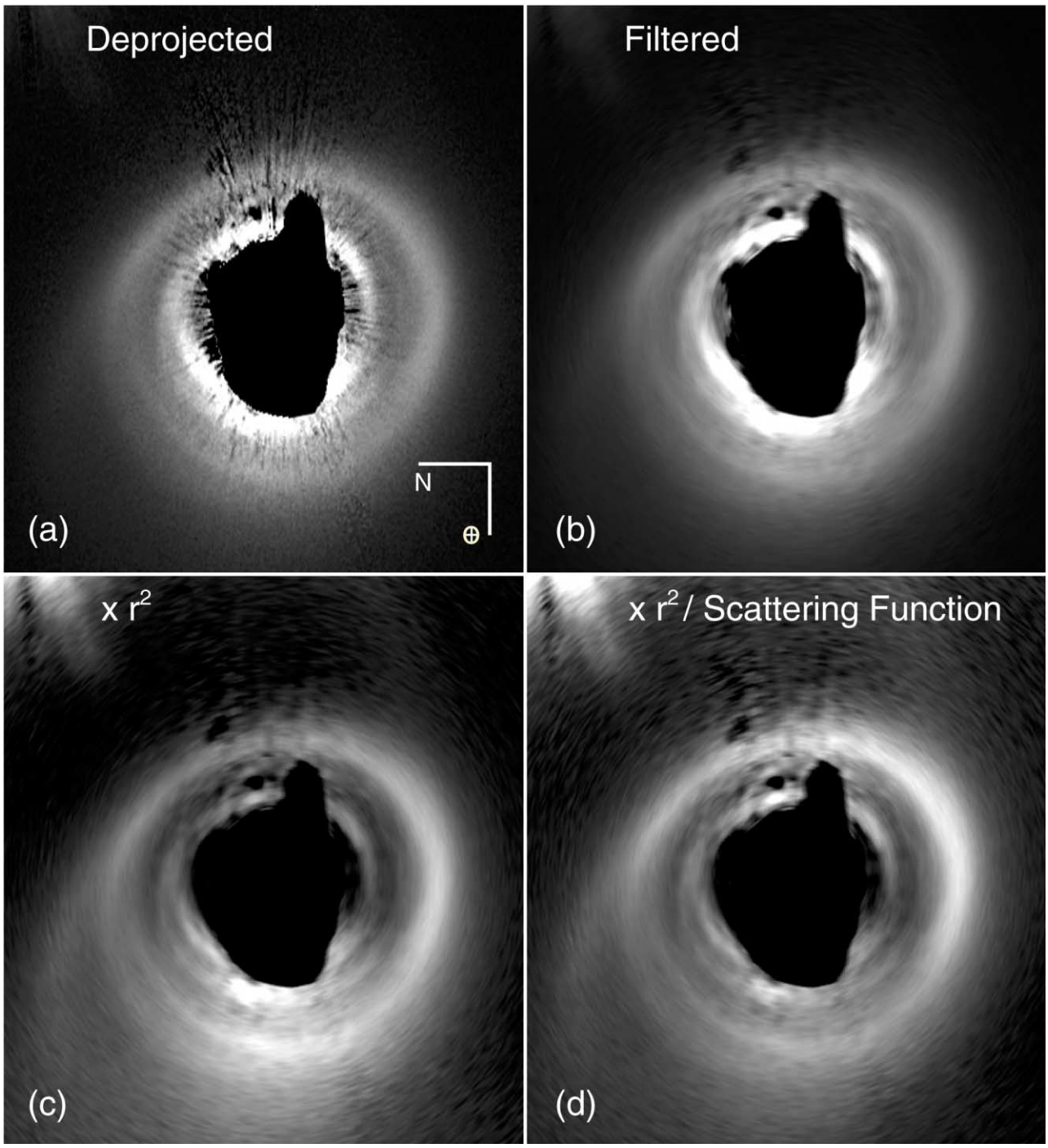

FIG. 7.—Sequence of images illustrating the derivation of a map of the disk's vertical optical depth. The line of sight is toward the bottom and north to the left. (*a*) Deprojected F435W + F606W image of the disk (square-root stretch). (*b*) Deprojected image after azimuthal median filtering (square-root stretch). (*c*) Azimuthally filtered image scaled to compensate for the inverse square drop in illumination by HD 141569A (linear stretch). (*d*) Image divided by a Henyey-Greenstein scattering asymmetry function with $g = 0.25$ (linear stretch). This image is proportional to the albedo times the optical depth perpendicular to the disk.

the observed color uniformity), Σ is $\sim$3 times greater in the southwest region of the outer ring than in the northeast. The peak of the apparent optical depth in the outer ring is $\omega\tau_{\perp} \approx 0.006$, assuming $g = 0.25$. W99 derived a mean $\omega\tau_{\perp} \approx 0.0036$ for the entire outer ring without correcting for forward scattering.

Because the HRC's occulting spots lie in the spherically aberrated beam from *HST*, some aberrated starlight passes by the spots and is corrected by the HRC optics. This corrected light forms a diminished image of the star on the detector within the imaged shadow of the spot (Fig. 1), which allows direct measurement of the star's position. (This technique was verified during postlaunch calibration of ACS.) Our images suggest that HD 141569A is not located at the center of the circumstellar disk. However, the disk's spiral structure precludes an accurate determination

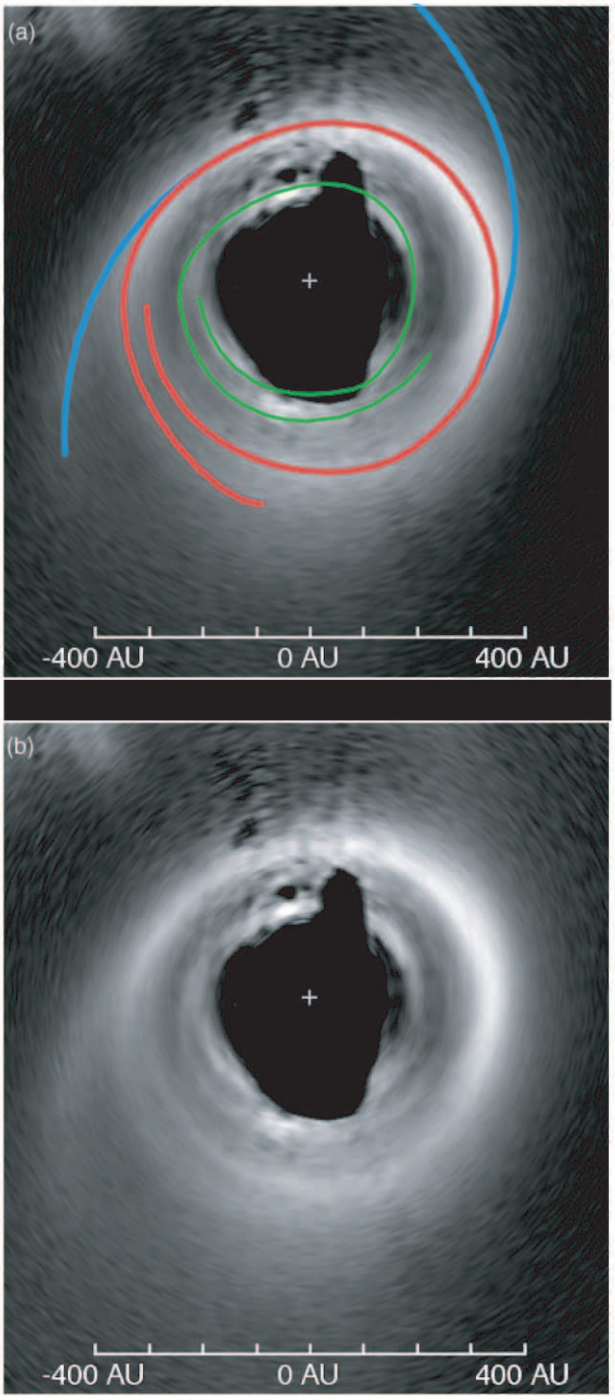

FIG. 8.—(*a*) Surface density with traced spirals: inner (*green*), outer (*red*), and open (*blue*). (*b*) Same image without traces. The disk orientation is the same as shown in Fig. 7.

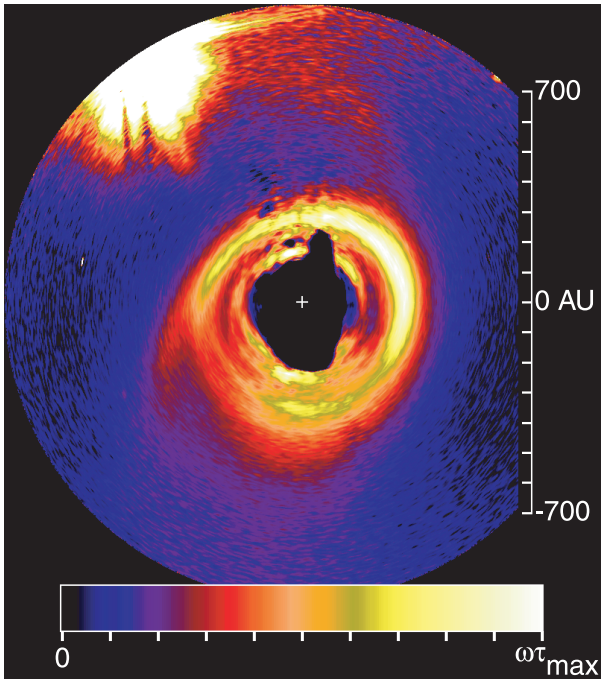

FIG. 9.—Color-coded map of the apparent optical depth (i.e., the product of the dust albedo ω and vertical optical depth $\tau_{\perp}$) of the HD 141569A disk. The image is normalized to the peak value in the outer ring ($\omega\tau_{\max} = 0.006$). The disk orientation is the same as that shown in Fig. 7. The plus sign marks the measured position of the star. The corrections for the r^{-2} illumination function and the scattering asymmetry make conspicuous the extended spiral structure of the disk.

of its center. The offset appears to be on the order of ~30 AU toward the west side of the disk, but the uncertainty in the measurement could exceed ~10 AU. An offset is also reported in STIS images of the disk (G. Schneider 2002, private communication). M01 did not report a star-to-disk offset in their STIS images, but they did note that the centers of the inner and outer rings are offset by 0.2 AU. We do not see an offset between the rings we show in Figure 8, although once again, the spiral structure complicates such a measurement.

4. DISCUSSION

Spiral structure has been observed in the circumstellar disk around HD 100546 (Grady et al. 2001), but that disk does not possess the open and extended spiral arms seen in HD 141569A's disk. The presence of these arms, the apparent association of the southwest arm with HD 141569BC, the large azimuthal density variations of the disk, and the ~25 AU offset of HD 141569A relative to the center of the disk are characteristics consistent with the tidal effects of encounters between circumstellar disks and passing stars (Pfalzner, Henning, & Kley 2000; Larwood & Kalas 2001). If HD 141569A and HD 141569BC are bound, then a few hundred encounters between the disk and HD 141569BC could have occurred over the 5 Myr age of the system. Under such circumstances, the disk would be tidally truncated at a distance of ~0.2–0.4 times the semimajor axis of the orbit and its outer regions would develop spiral structure (Artymowicz & Lubow 1994). The eccentricity of the HD 141569A-BC system would also induce eccentricity in the disk that could account for the displacement of the disk with respect to HD 141569A. Detailed dynamical modeling of the system is required to explore fully the possible interaction of the disk with HD 141569BC.

The redness of the disk relative to HD 141569A indicates that the grain properties are different from those of the neutrally colored but older disk around β Pic. However, the color of HD 141569A's disk is similar to HR 4796A's disk (Schneider & Silverstone 2002) and indicates that the scattering efficiency of the dust increases with wavelength. While our images cannot strongly constrain the distribution and size of the dust grains, they do permit quantitative

speculation. For example, a reasonable match to the observed colors is obtained if we assume that the grains are composed of "astronomical silicate" (Laor & Draine 1993; Draine & Lee 1984) and that the distribution of grain sizes obeys a power law with an index of 3.5 and radi extrema of 0.4 and 10 μm. These assumptions imply a V-band albedo of $\omega \approx 0.6$. Other combinations of the grain composition, size distribution, and albedo may, however, produce equally good matches to the observed disk colors. Nevertheless, the size distribution quoted above is consistent with that derived by A99 from the disk's 8–100 μm spectral energy distribution and an assumed composition of silicate grains, organic refractories, and water ice.

The spatial uniformity of the disk's color does not necessarily imply that the distribution of grain sizes is constant throughout the disk. The colors are not sensitive to the distribution of grains with sizes $\gtrsim 5$ μm. Therefore, color uniformity alone is not inconsistent with the scenario of dust segregation in the presence of stellar radiation pressure (Takeuchi & Artymowicz 2001). However, the azimuthally varying density distribution of the grains (Fig. 9) and the protracted timescale of such segregation relative to possible periodic encounters with HD 141569BC make dust segregation an unlikely cause of the observed disk structure.

The complex structure of the disk prompts us to reconsider the potential influence of a very low mass companion on the disk's morphology. W99 have suggested that the depleted region of the disk from ~215 to 300 AU could be produced by tidal clearing by a Jupiter-sized planet in the gap itself. Takeuchi & Artymowicz (2001) and Klahr & Lin (2002) have argued that the arcs seen in the disks around HR 4796A and HD 141569A may not necessarily be indicators of embedded planets. Current theories suggest that planet formation at such large distances from HD 141569A is unlikely within 5 Myr (Boss 1998). Moreover, Takeuchi & Artymowicz (2001) argue that the creation of a circular depleted region by an outwardly migrating planet is unlikely. Alternatively, HD 141569BC may have induced the scattering of a planet from a small orbit to the gap. Thommes, Duncan, & Levison (2002) have also shown that planets within 100 AU may scatter objects out to 300 AU. Whether the orbit of a scattered planet within HD 141569A's disk could circularize within 5 Myr is unclear. On the other hand, the cause of the gap need not be in the gap itself; a planet in a close orbit might clear the gap via excited density waves within its outer Lindblad resonance (Goldreich & Tremaine 1978). Indeed, Brittain & Rettig (2002) have presented evidence for H_3^+ within 17 AU of HD 141569A, which may be attributed to the extended envelope of a protoplanet. All these possibilities remain to be investigated. Our images do not exclude a planet as the mechanism responsible for some of the disk's structure.

The causes of the complicated structures observed in the dust disks around HD 141569A and other young stars clearly require further investigation and modeling. As our images demonstrate, the ACS coronagraph can produce images of these disks with unprecedented resolution and contrast. Such high-quality images permit the type of studies necessary to address quantitatively the many outstanding questions regarding the composition, dynamics, and evolution of protoplanetary disks.

We are grateful to P. Artymowicz, S. Lubow, J. Pringle, and D. Lin for discussions about dynamical modeling, to G. Schneider for details of prior *HST* STIS observations, and to H. Throop for help with the dust scattering models. We also thank T. Allen, K. Anderson, S. Barkhouser, S. Busching, A. Framarini, D. Magee, and W. J. McCann for their invaluable contributions to the ACS Investigation Definition Team (IDT) and Christine Klicka for assistance with the graphics. This work was supported by NASA grant NAG 5-7697 to the ACS IDT.

REFERENCES

Artymowicz, P., & Lubow, S. H. 1994, ApJ, 421, 651
Augereau, J. C., Lagrange, A. M., Mouillet, D., & Ménard, F. 1999, A&A, 350, L51 (A99)
Boss, A. P. 1998, ApJ, 503, 923
Brittain, S. D., & Rettig, T. W. 2002, Nature, 418, 57
de Winter, D., van den Ancker, M. E., Maira, A., Thé, P. S., Djie, H. R. E. T. A., Redondo, I., Eiroa, C., & Molster, F. J. 2001, A&A, 380, 609
Draine, B. T., & Lee, H. M. 1984, ApJ, 285, 89
ESA. 1997, The Hipparcos and Tycho Catalogues (ESA SP-1200) (Noordwijk: ESA)
Fisher, R. S., Telesco, C. M., Piña, R. K., Knacke, R. F., & Wyatt, M. C. 2000, ApJ, 532, L141
Goldreich, P. & Tremaine, S. D. 1978, Icarus, 34, 240
Grady, C. A., et al. 2001, AJ, 122, 3396
Henyey, L. G., & Greenstein, J. L. 1941, ApJ, 93, 70
Hoffleit, D., & Jaschek, C. 1982, The Bright Star Catalogue (4th rev. ed.; New Haven: Yale Univ. Obs.)
Jaschek, C., & Jaschek, M. 1992, A&AS, 95, 535
Jaschek, M., Jaschek, C., & Egret, D. 1986, A&A, 158, 325
Klahr, H. H., & Lin, D. N. C. 2000, ApJ, 554, 1095
Krist, J. E., Hartig, G. F., Clampin, M., Golimowski, D. A., Ford, H. C., & Illingworth, G. D. 2002, Proc. SPIE, 4860, 20
Laor, A., & Draine, B. T. 1993, ApJ, 402, 441
Larwood, J. D., & Kalas, P. G. 2001, MNRAS, 323, 402
Mouillet, D., Lagrange, A. M., Augereau, J. C., & Ménard, F. 2001, A&A, 372, L61 (M01)
Oudmaijer, R. D., et al. 2001, A&A, 379, 564
Pavlovsky, C., et al. 2002, Advanced Camera for Surveys Instrument Handbook (ver. 3.0; Baltimore: STScI)
Pfalzner, S., Henning, T., & Kley, W. 2000, Birth and Evolution of Binary Stars, ed. B. Reipurth & H. Zinnecker (Potsdam: Astrophys. Inst. Potsdam), 193
Schneider, G., & Silverstone, M. 2002, in ASP Conf. Ser. 291, *Hubble*'s Science Legacy, ed. K. R. Sembach, J. C. Blades, G. D. Illingworth, & R. C. Kennicutt. Jr. (San Francisco: ASP), 69
Sylvester, R. J., Skinner, C. J., Barlow, M. J., Mannings, V. 1996, MNRAS, 279, 915
Takeuchi, T., & Artymowicz, P. 2001, ApJ, 557, 990
Thommes, E. W., Duncan, M. J., & Levison, H. F. 2002, AJ, 123, 2862
Weinberger, A. J., Becklin, E. E., Schneider, G., Smith, B. A., Lowrance, P. J., Silverstone, M. D., Zuckerman, B., & Terrile, R. J. 1999, ApJ, 525, L53 (W99)
Weinberger, A. J., Rich, R. M., Becklin, E. E., Zuckerman, B., & Matthews, K. 2000, ApJ, 544, 937